Article

Enhanced Solar Water Desalination by $CuCo_2S_4$-decorated Carbon Foam Derived from Waste Plastics

Muzammil HUSSAIN[1,2], Tofik Ahmed SHIFA[1]✉, Pratik V. SHINDE[1], Pankaj KUMAR[4], Stefano CENTENARO[1,5], Silvia GROSS[3], Elisa MORETTI[1] and Alberto VOMIERO[1,4]✉

Received April 12, 2024
Accepted May 15, 2024

Interfacial solar desalination is an emerging technology for freshwater production, but the finding of novel solar evaporators is still challenging. In the present research, graphitic carbon foam (CF) was synthesized from the upcycling of waste plastic polyethylene terephthalate (PET) waste bottles functionalized with carrollite $CuCo_2S_4$ as a photothermal layer. Analytical characterization [X-ray diffraction (XRD), Fourier transform infrared spectroscopy (FTIR), and scanning electron microscopy-energy dispersive spectroscopy (SEM-EDS)] confirms the functionalization of carrollite $CuCo_2S_4$ on graphitic carbon foam. The UV-Vis spectroscopy analysis showed an enhanced optical absorption in the UV-Vis-near IR region (>96%) for functionalized $CuCo_2S_4$-CF foam compared to carbon foam (67%). The interfacial solar desalination experiment presented a significantly enhanced evaporation rate of 2.4 $kg·m^{-2}·h^{-1}$ for $CuCo_2S_4$-CF compared to that of CF (1.60 $kg·m^{-2}·h^{-1}$) and that of $CuCo_2S_4$ (1.60 $kg·m^{-2}·h^{-1}$). The obtained results proved that the newly synthesized $CuCo_2S_4$-CF from the upcycled plastic into new material for the photothermal desalination process can enhance the practice of a circular economy to produce fresh water.

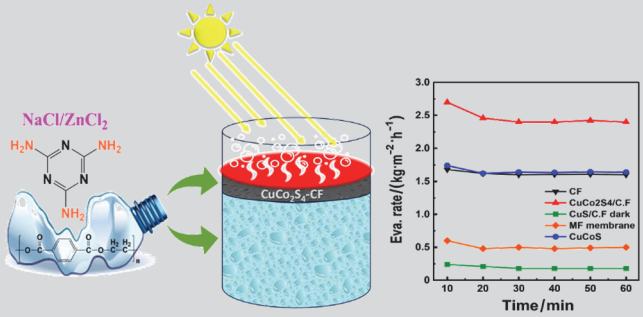

Keywords Photothermal desalination; Cobalt; Copper; Chalcogenide; Waste upcycling; Circular economy

1 Introduction

Water is the most essential need for all living organisms, but with the limited resources of freshwater and increasing commercial and industrial sectors, freshwater availability is under high threat. Water desalination of widely available seawater resources will significantly help to fill the gap of water shortage with techniques, such as membrane desalination, thermal desalination, and emerging desalination. However, these techniques are still not favorable due to energy consumption and environmental impact.[1] Solar energy is the most cost-effective source of renewable energy, and interfacial solar desalination has gained much attention in water management.

To enhance the evaporation rate, the engineering of the interfacial solar evaporators relies on two major factors: a solar absorber and a substrate.[2] For enhanced evaporation rate, the ideal solar absorber should absorb maximum solar radiation and convert it into thermal energy, and an efficient substrate should be highly hydrophilic and prevent thermal energy loss.[3,4] Moreover, a material for interfacial solar desalination should be cost-effective with as low as possible environmental impact. For this reason, recently some carbon-based materials, such as graphene oxide,[5,6] graphene aerogel,[7] and carbon nanotubes (CNTs)[8] have been reported for solar desalination. Unfortunately, these materials are not very efficient due to low solar-to-thermal conversion, low evaporation rate, and high cost of production for materials, such as graphene aerogel.

Therefore, considering the sustainability goals, waste plastics can be a good raw material to upcycle into new viable material and to enable the circular economy.[9] In fact, it is one of the major causes of the global white pollution crisis, because most of the plastics end up as waste, polluting the environment. According to a recent environmental survey, global greenhouse gas emissions would grow by 31% from 2015 to the end of 2030.[10] To deal with this ever-increasing environmental issue, various strategies, such

✉ Alberto VOMIERO
alberto.vomiero@ltu.se
✉ Tofik Ahmed SHIFA
tofikahmed.shifa@unive.it
1. Department of Molecular Sciences and Nanosystems, Ca' Foscari University of Venice, Via Torino 155, 30172 Venice, Italy;
2. Department of Industrial Engineering, University of Padova, Via Venezia 1, 35131 Padova, Italy;
3. Department of Chemical Sciences, University of Padova, Via Francesco Marzolo 1, 35131 Padova, Italy;
4. Division of Materials Science, Department of Engineering Sciences and Mathematics, Luleå University of Technology, 97187 Luleå, Sweden;
5. Center for Cultural Heritage Technologies (CCHT), Istituto Italiano di Tecnologia (IIT), Via Torino 155, 30170 Venezia-Mestre, Italy

as landfill, mechanical, and chemical recycling, and incineration were adopted. However, landfill and incineration faced much criticism due to production of secondary pollutants, while mechanical and chemical recycling got much attention for reducing greenhouse gases. Recently some studies have been reported for the upcycling of waste plastic into carbon foam (CF) for interfacial solar desalination that provided a significantly enhanced evaporation rate,[11−13] compared to other carbon-based materials, such as graphene, carbon nanotube (CNT) and carbonized carbon black. Carbon foam has appealing characteristics, such as porous structure and rough morphology, low thermal conductivity, and high water transport due to porous microchannels.[11]

In the past decades, the semiconductor functionalized carbon materials have been intensively studied for photocatalytic, photovoltage, and synergetic functions of photothermal applications.[14] Recently, cobalt and copper-based nanostructures, such as Co_3O_4@PDA-rGO (GO: graphene oxide), $CoSb_3$, Co@C/NCNT (NCNT: nitrogen-doped carbon nanotube), cuprous telluride, and Cu-GO/ gained much attention for photothermal applications due to localized surface plasmonic resonance.[15−19] Furthermore, sulfide-based materials are extensively studied for numerous energy and environmental applications, where the engineering of nanostructures plays a key role in catalyst performance.[20−23] The ternary cobalt copper sulfide (Co_2CuS_4), a thiospinel nanostructure, has been recently studied for its excellent performance for supercapacitors, solar cells, lithium-ion batteries. The appealing thermal stability, and controllable morphology of $CuCo_2S_4$ makes it an excellent candidate for photocatalytic applications in dye degradation and hydrogen evolution.[24−27]

In the present research work (Fig. 1), we upcycled the waste polyethylene terephthalate (PET) material into graphitic CF and further functionalized it with carrollite $CuCo_2S_4$. The rationale for focusing on carrolite is due to its excellent track record in photocatalytic pollutant degradation,[26] hydrogen evolution,[27] and photothermal application.[28] Despite these applications, it has not yet been reported as an active material for interfacial solar desalination. Accordingly, we controllably synthesized $CuCo_2S_4$ and integrated it with CF upcycled from environmental plastic wastes and obtained an excellent result that can be substantiated by the enhanced evaporation rate and surface temperature. This work aligns with the global circular economy and gives a fresh insight into the sustainable development of photo-active material for interfacial solar desalination to produce clean water.

2 Experimental

2.1 Reagent and Chemicals

All the chemicals and reagents used in this research work, such as $Cu(NO_3)_2{\cdot}3H_2O$, $Co(NO_3)_2{\cdot}6H_2O$, NH_4OH, NaCl, $ZnCl_2$, melamine, HCl, and thiourea were purchased from Sigma Aldrich.

2.2 Synthesis of $CuCo_2S_4$-CF

Initially, CF was synthesized by following the already reported procedure: [11] 1.5 g of waste PET bottle sheets were mixed with 3 g of eutectic salt [$ZnCl_2$/NaCl (58/42, mass ratio)], and 0.75 g of melamine. Then the mixture was placed in the muffle furnace and calcined at 340 °C for 30 min with a heating rate of 10 °C/min. After cooling to room temperature, the obtained black foam was mashed and washed using dilute HCl and deionized water repeatedly till neutral pH. Finally, the obtained carbon foam powder was dried in an oven at 50 °C overnight, packed, and labeled as CF. The solvothermal method was used to grow $CuCo_2S_4$ on the CF powder: in detail, 0.75 mmol of $Cu(NO_3)_2{\cdot}3H_2O$ and 1.5 mmol of $Co(NO_3)_2{\cdot}6H_2O$ were dissolved in 10 mL of distilled water followed by the addition of 0.15 g of CF powder, and then 25 mL of ethanol was added and sonicated for 20 min. Then the mixture solution (pH 9) was maintained using ammonium hydroxide at room temperature with continuous stirring, as the mixture attained greenish color, 0.228 g of thiourea was added and the reaction continued for 12 h at 80 °C. The suspension mixture was transferred into a Teflon-lined stainless-steel autoclave and heated at 180 °C for 6 h. Finally, the obtained black powder was centrifuged and

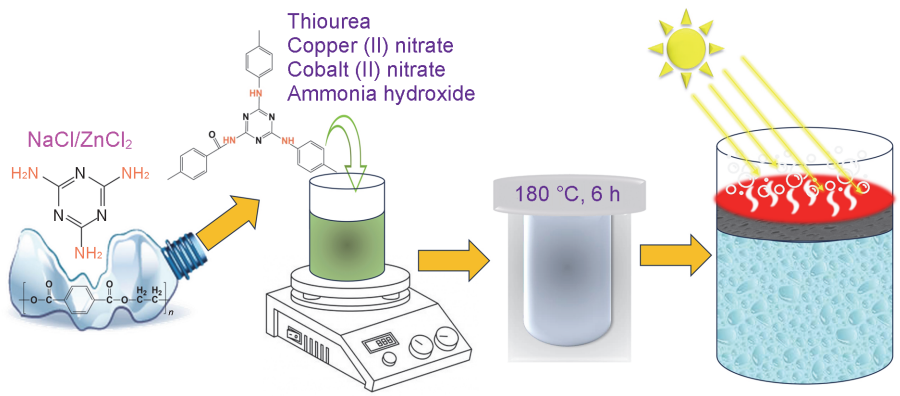

Fig. 1 Graphical synthesis illustration of CF and functionalization with carrollite $CuCo_2S_4$ on CF powder for interfacial solar desalination

https://doi.org/10.1007/s40242-024-4091-8

washed with deionized water and ethanol, and the powder material was dried at 60 °C overnight. The pure $CuCo_2S_4$ was also prepared by using the same methodology without the addition of CF powder.

2.3 Characterization

The X-ray diffraction (XRD) analysis was performed using a Philips PW1050/37 diffractometer. The UV-Vis absorption spectroscopy measurements were carried out with an ultraviolet-visible spectrophotometer LAMBDA 1050+, Perkin Elmer with an integrating sphere. The scanning electron microscopy-energy dispersive spectroscopy (SEM-EDS) analysis was carried out using an FEI Magellan 400 FEG-SEM with an EDS detector (X-Max 80 mm^2 SDD, Oxford Instrument). The IR absorption spectrum was recorded with an Fourier transform infrared spectroscopy (FTIR) spectrometer (Nicolet 6700 FTIR Spectrometer) in transmission mode. The contact angle measurements were performed using an FTA 1000 Analyzer System. X-Ray photoelectron spectroscopy (XPS) was performed using an ESCALAB 250 (ThermoFisher Scientific, USA) with X-ray source monochromated Al $K\alpha$, 150 W, 1486.6 eV, and energy pass of 200 eV for the survey and 30 eV for high-resolution scans.

2.4 Interfacial Solar Evaporation

For the interfacial solar desalination experiment, 0.1 g of powdered material of CF powder, $CuCo_2S_4$, and $CuCo_2S_4$-CF was sonicated for 5 min in 20 mL of deionized water and deposited separately on a glass microfiber filter (Whatman GF/F, CAT No. 1825-047) using vacuum filtration assembly. The membrane after the deposition of the material was dried at 60 °C. Then 40 mL of brine solution [0.6 mol/L NaCl solution in the deionized water that is 3.5% (mass fraction) average global seawater salinity] in a 50 mL beaker with a cotton sponge that facilitated saline water transport and polyethylene foam as a thermal insulator was used to cover beaker. Finally, the experiment for evaporation rate was conducted under one sun radiation (air mass 1.5 global, AM1.5G, 100 W/cm^2) by placing a 1 cm×1 cm prepared membrane on a carbon sponge. The surface temperature of the membrane was recorded using a thermal camera (FLIR C3-X) for both the dry and wet stages. The change in mass was calculated by using an analytical balance and the solar evaporation rate was calculated with the following equation:

$$\text{Evaporation rate} = \frac{\Delta m}{S} \times \tau$$

where Δm is the mass loss of water (kg), S is the area of the evaporation (m^2), and τ is the evaporation time (h).

3 Results and Discussion

3.1 Characterization

3.1.1 XRD Analysis

The as-synthesized graphitic CF, $CuCo_2S_4$, and $CuCo_2S_4$ decorated CF powder were characterized by XRD over the angular range (10°—80°) to examine their phase and crystal structure. The diffraction peaks for CF (Fig. 2A) show the corresponding diffraction plane (002) (JACPDs: 41-1487) that indicated the graphitic structure of synthesized CF. The broad peak in the 2θ range of 18°—32° pertains to reflection from (002) plane.[11] The XRD patterns of $CuCo_2S_4$ and $CuCo_2S_4$-CF exhibit peaks at 2θ=16.1°, 26.5°, 31.27°, 37.96°, 46.99°, and 49.96°, corresponding to crystal planes (111), (022), (113), (004), (224), and (115) of carrolite (JCPDS: 42-1450) (Fig. 2B). It is important to note that both $CuCo_2S_4$ and $CuCo_2S_4$-CF resulted in a similar XRD pattern, suggesting that CF as matrix does not affect the growth of carrollite $CuCo_2S_4$.

3.1.2 SEM Analysis

The surface morphologies of the synthesized graphitic CF powder, $CuCo_2S_4$, and $CuCo_2S_4$-CF were analyzed at different magnifications. The SEM images of graphitic CF present the open-cell interconnected pores on the surface that were generated due to the physical template of molten salt (Fig. 3). Similar surface morphology has been reported in a recent investigation for waste plastic-derived CF.[13]

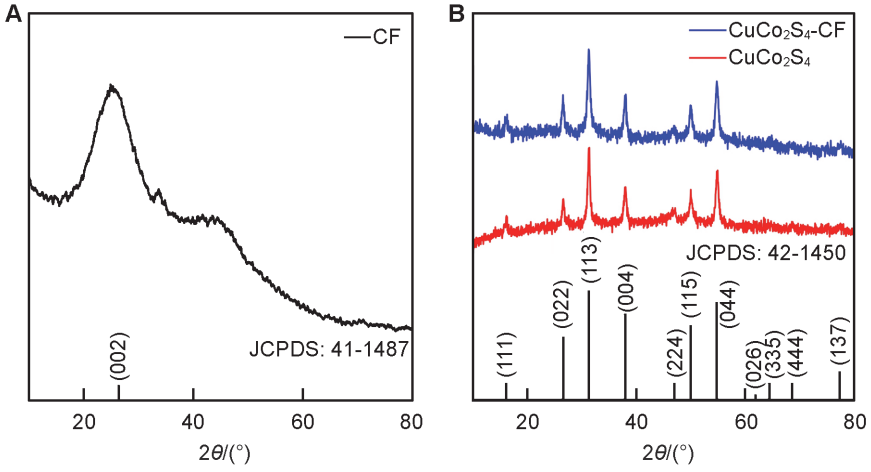

Fig. 2 XRD patterns of graphitic CF (A), and $CuCo_2S_4$ and $CuCo_2S_4$-CF (B)

https://doi.org/10.1007/s40242-024-4091-8

Moreover, the flat sheet presents the existence of multilayer graphitic sheets in the architecture of CF and these results show good agreement with the reported morphology of CF.[12,29] The SEM images for the $CuCo_2S_4$ show the agglomerated nanobeads like morphology (Fig. S1, in the Electronic Supplementary Information, ESI) and similar nanobeads were illustrated for $CuCo_2S_4$-CF that clearly present the no effect on morphology with functionalization of $CuCo_2S_4$ on CF matrix (Fig. 3). The elemental compositions of CF, $CuCo_2S_4$, and $CuCo_2S_4$-CF were investigated using EDS equipped with FE-SEM. EDS spectra show the elemental composition of sample CF (Fig. 3, carbon, nitrogen, oxygen), $CuCo_2S_4$ (Fig. S1, copper, cobalt, sulfur), $CuCo_2S_4$-CF (Fig. 4, carbon, nitrogen, oxygen, copper, cobalt, sulfur) and elemental mapping shows the uniformity of elemental distribution on CF matrix.

3.1.3 FTIR Analysis

The FTIR analysis was performed to analyze the functional group/bonding nature of the as-synthesized CF and $CuCo_2S_4$-CF (Fig. 5A). The stretching vibration of —OH and the asymmetric stretching vibration peaks are observed at 3430 cm^{-1}. The stretching vibration of C—H and COOH is responsible for the peaks at 3200 and 1720 cm^{-1}, respectively. The peaks appearing at 1630 and 1380 cm^{-1} correspond to C═N stretching vibration and benzene stretching vibration. The obtained FTIR spectrum for the synthesized CF agrees with the recently reported spectrum of carbon foam.[11] In the case of functionalized CF with $CuCo_2S_4$, the additional peaks at 617 and 475 cm^{-1} correspond to symmetric and asymmetric stretching vibrations of Cu—S, and Co—S and similar observation has already been

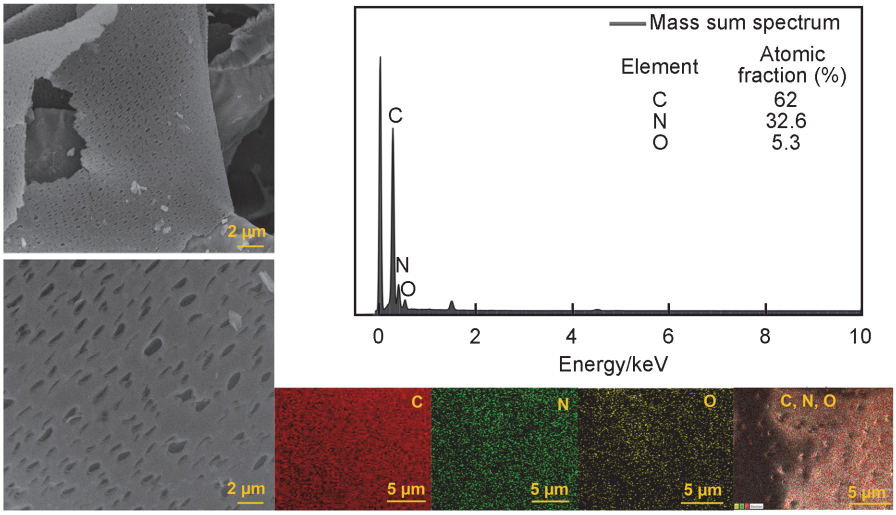

Fig. 3 SEM-EDS analysis of CF

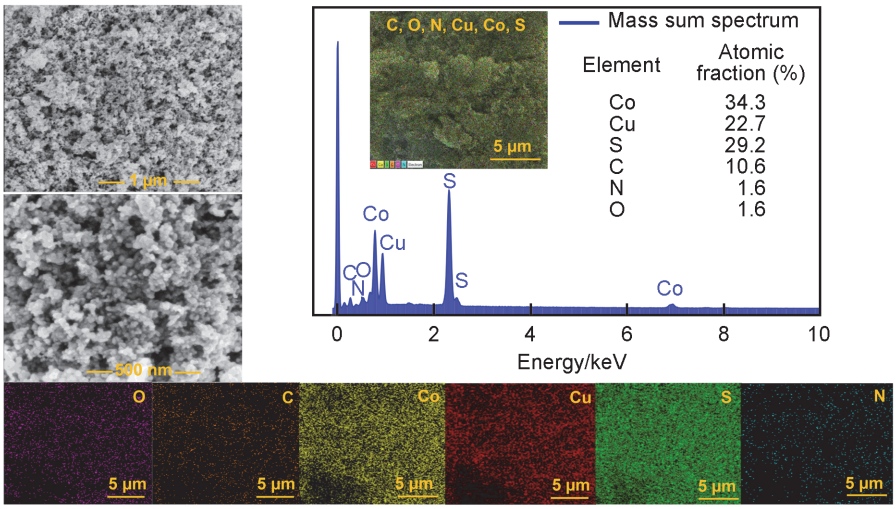

Fig. 4 SEM-EDS analysis of $CuCo_2S_4$-CF

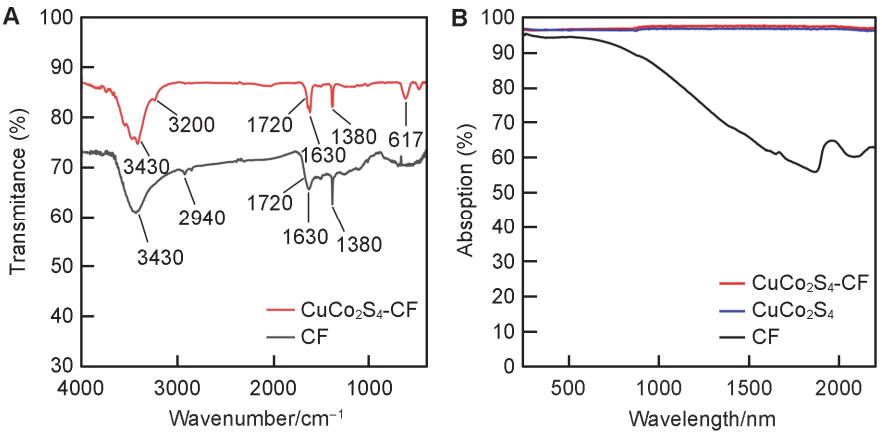

Fig. 5 FTIR spectra of CF and $CuCo_2S_4$-CF (A) and absorption spectra of CF, $CuCo_2S_4$, and $CuCo_2S_4$-CF (B)

https://doi.org/10.1007/s40242-024-4091-8

reported for $CuCo_2S_4$.[30]

3.1.4 XPS Analysis

XPS was performed to analyze the chemical composition of the synthesized CF, $CuCo_2S_4$, and $CuCo_2S_4$-CF. The XPS survey indicates the presence of C, N, and O in sample CF (Fig. S2, A and E in the ESI). The obtained binding energies of C 1*s* (deconvoluted peaks: C—N 288 eV, C═N 286.3 eV, and graphitic carbon C—C 284.8 eV), N 1*s* (graphitic N 400.2 eV and pyridinic N 398.7 eV), and O 1*s* (COOH 533 eV, and C—O 531.5 eV) confirmed the graphitic character of CF (Fig. S2, B—D). The obtained results matched well with the reported binding energies of C 1*s*, N 1*s* and O 1*s* for CF.[11] The XPS spectrum in Fig. S2E shows the presence of Cu, Co, and S for the carrolite $CuCo_2S_4$. The XPS survey spectrum for the $CuCo_2S_4$ functionalized CF indicates the presence of C, N, O, Cu, Co, and S (Fig. 6A). The obtained binding energies for the deconvoluted peaks of C 1*s*, N 1*s*, and O 1*s* are the same as those in the bare CF sample. The binding energies for the Cu [$2p_{2/3}$ (932.7 eV) and $2p_{1/2}$ (952.2 eV)], Co 2*p* [$2p_{1/2}$ (793.8 eV) and $2p_{2/3}$ (779.6 eV)] and S [$2p_{3/2}$ (161.7 eV) and $2p_{1/2}$ (162.8)] are similar as those in the pristine sample in Fig. 6, B—G. The obtained results confirm that the functionalization of CF with carrolite $CuCo_2S_4$ does not affect the graphitic structure of CF and CF does not affect the phase purity of carrolite $CuCo_2S_4$.

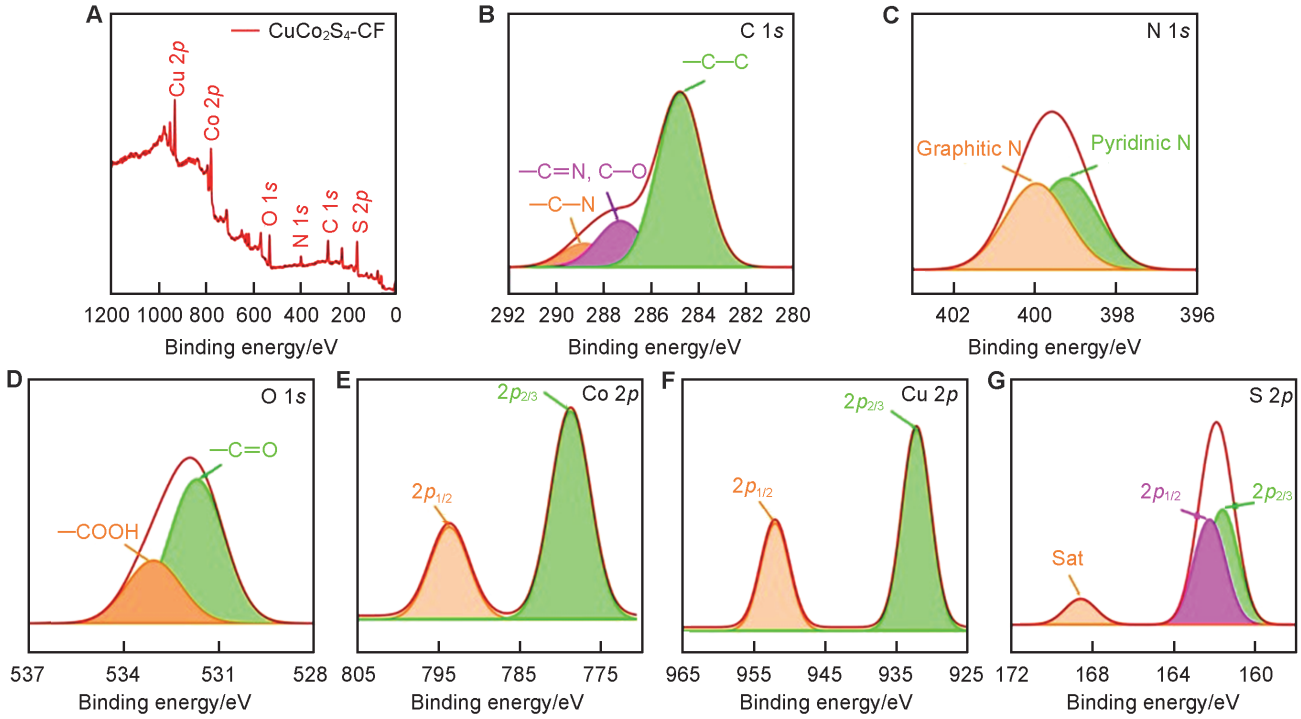

Fig. 6 XPS analysis of $CuCo_2S_4$-CF

(A) Survey XPS spectrum of $CuCo_2S_4$-CF; (B) C 1*s*; (C) N 1*s*; (D) O 1*s*; (E) Co 2*p*; (F) Cu 2*p*; (G) S 2*p*. Spectra were corrected for changing effect.

3.2 Optical Properties of $CuCo_2S_4$-CF

To monitor the potentiality of the material as solar evaporator, UV-Vis absorption spectroscopy was applied in the spectral range of 250—2200 nm. Fig. 5B shows the absorption for all the samples. For the bare CF, absorbance is equal to 95% in the UV-Vis region. However, moving from the Vis to the near IR and IR regions, the solar absorption decreased down to 55% at 1800 nm. This trend is in accordance with other reported studies on CF powder.[12] To enhance the evaporation rate for the interfacial solar desalination process, the solar evaporators should absorb maximum solar radiation in the near IR region. A recent study shows that ternary $CuCo_2S_4$ has excellent photothermal activity, giving rise to strong absorption that ranges from UV-Vis to near IR.[28] Based on these findings, we functionalized the CF with $CuCo_2S_4$ to realize enhanced light absorption that extends to the IR region. To this end, the obtained material presents excellent absorption above 96% in the UV-Vis-IR region (Fig. 5B). Based on the obtained characterization results, CF shows micropores with a graphitic structure that may facilitate water transport, and functionalization with $CuCo_2S_4$ nanoparticles, which may enhance the optical absorption of the system to harvest maximum solar energy. For these reasons, it is expected that $CuCo_2S_4$-CF can work as an excellent solar evaporator.

3.3 Interfacial Solar Desalination

The solar evaporation experiment was conducted to measure the evaporation rate of $CuCo_2S_4$-CF. For comparison, the pure $CuCo_2S_4$, CF, and microfiber membrane (Whatman glass microfiber filter: 47 mm) were also reported separately. The dry surface temperatures of CF, $CuCo_2S_4$, and $CuCo_2S_4$-CF are reported in Fig. 7, resulting in 68 °C for CF, 70.6 °C for $CuCo_2S_4$, and 74.4 °C for $CuCo_2S_4$-CF. The wet surface temperatures were recorded as 41, 39 and 43.8 °C for CF, $CuCo_2S_4$, and $CuCo_2S_4$-CF, respectively (Fig. S3 in the ESI). The comparison of the dry and wet surface temperature of the samples is presented in Fig. S4 in the ESI. It is observed that, in both cases, the temperature under dry and wet conditions of the $CuCo_2S_4$-CF sample is higher than that of the other samples, most likely due to the photothermal effect of $CuCo_2S_4$ and low thermal conductivity of carbon foam that prevents heat losses. The interfacial solar desalination experiment shows the enhanced evaporation rate (2.40 $kg·m^{-2}·h^{-1}$) for the $CuCo_2S_4$ functionalized CF compared to CF (1.6 $kg·m^{-2}·h^{-1}$) and $CuCo_2S_4$ (1.6 $kg·m^{-2}·h^{-1}$) (Fig. 8B). The evaporation rate of $CuCo_2S_4$-CF under dark conditions (no solar irradiation) shows an evaporation rate of 0.18 $kg·m^{-2}·h^{-1}$ that is even lower than the evaporation rate for microfiber membrane (0.5 $kg·m^{-2}·h^{-1}$). For enhanced evaporation rate, the morphology of the material plays a key role. The SEM analysis shows the carbon surface with micropores that facilitate the capillary action of water transport towards the photothermal layer. The 3D connected graphitic structure can prevent heat loss. The continuous change in mass reduction (kg/m^2) shows the hydrophilicity of synthesized $CuCo_2S_4$-CF due to the faster movement of water toward the photothermal layer (Fig. 8A), and the investigation of CF for interfacial solar desalination showed excellent salt-resistant property.[11] Fig. 9 shows the

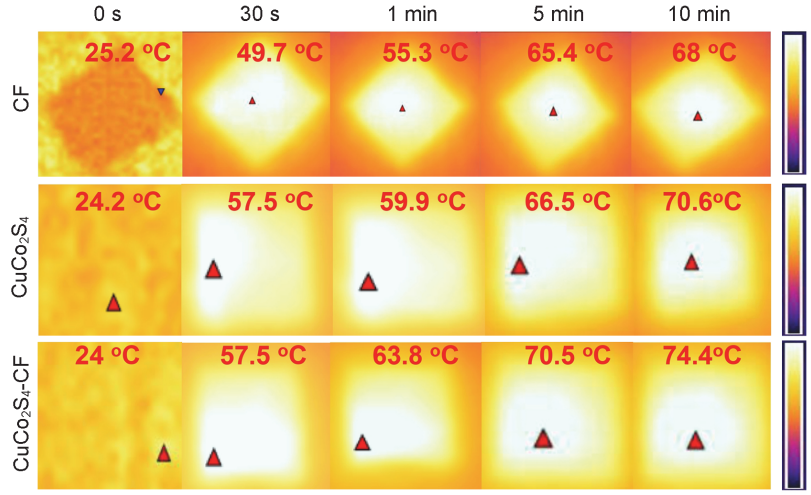

Fig. 7 Comparison of the dry surface temperature of CF, $CuCo_2S_4$, and $CuCo_2S_4$-CF

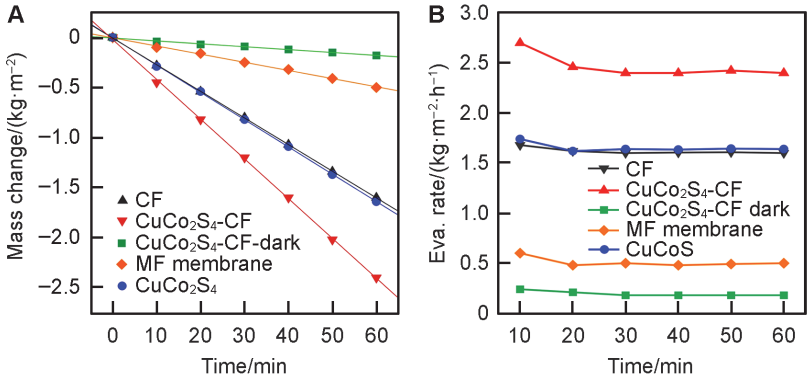

Fig. 8 Change in mass (A) and evaporation rate (B) of CF, $CuCo_2S_4$, and $CuCo_2S_4$-CF

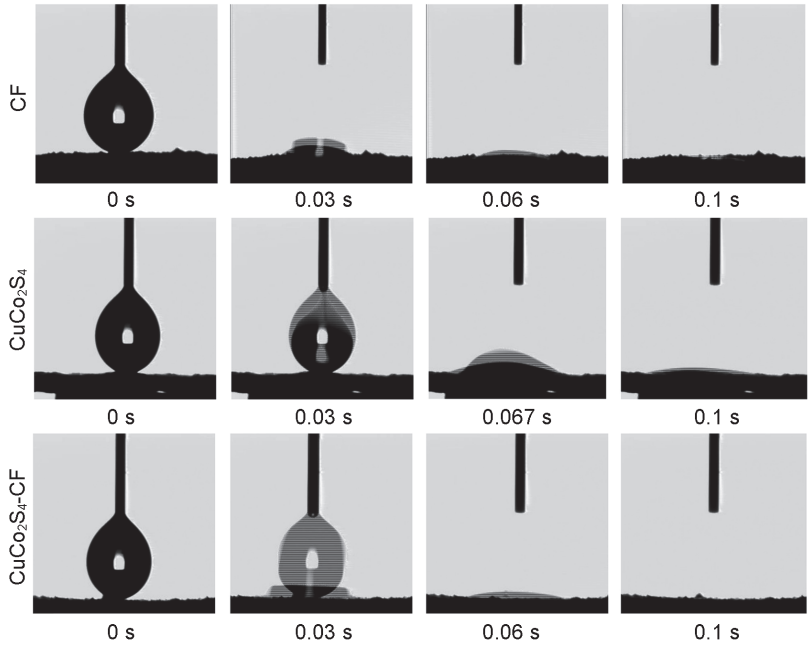

Fig. 9 Contact angle measurements of CF, $CuCo_2S_4$ and $CuCo_2S_4$-CF

https://doi.org/10.1007/s40242-024-4091-8

hydrophilicity of synthesized CF, $CuCo_2S_4$, and $CuCo_2S_4$-CF, which was analyzed with contact angle measurements and it shows very high hydrophilicity of $CuCo_2S_4$ functionalized CF. The water drop absorbs within 0.1 s in the case of both CF and $CuCo_2S_4$-CF, proving the super hydrophilicity of material due to the presence of O-, N-containing functional groups in graphitic CF. The functionalization with $CuCo_2S_4$ does not affect the hydrophilicity of the material.

The evaporation rate of CF (1.60 $kg·m^{-2}·h^{-1}$) well matched with a reported evaporation rate of carbon foam.[13] the evaporation rates for $CuCo_2S_4$ (1.62 $kg·m^{-2}·h^{-1}$) and $CuCo_2S_4$-CF (2.40 $kg·m^{-2}·h^{-1}$) have never been investigated before, except in the present research work. The evaporation rate for $CuCo_2S_4$-CF has achieved a significantly higher value, compared to recently reported studies on carbon-based, copper, and cobalt-based nano photothermal evaporators (Table 1).[13,16,31—36] The mechanism behind the enhanced evaporation seems being the combined effect of graphitic CF with porous channels that facilitate fast water transport, preventing at the same time heat losses, and the solar absorption in a broadband, thanks to the narrow band gap of the $CuCo_2S_4$-CF photothermal layer.

Table 1 Comparison of the evaporation rate for $CuCo_2S_4$-CF with different C-, Cu-, and Co-based solar evaporators

Photothermal material	Evaporation rate/ ($kg·m^{-2}·h^{-1}$)	Surface temperature/ºC	Ref.
CF/PVDF	1.27	75	[13]
$CoSb_x$	1.4	101	[16]
CuS nanoflower	1.09	35	[31]
Chitin/CuS composite	1.52	84.1	[32]
Cu_2SnSe_3	1.62	40.1	[33]
Wood CNT	0.95	36.2	[34]
Co_3S_4	1.26	38	[35]
Co_3S_4/NF	1.56	40	[36]
$CuCo_2S_4$-CF	2.40	74.4	This work

4 Conclusions

In the present research work, the newly combined nanostructure of $CuCo_2S_4$-CF was synthesized by upcycling the waste plastic into graphitic CF, and $CuCo_2S_4$ was functionalized on the CF powder using solvothermal techniques. Carrollite $CuCo_2S_4$ functionalized CF showed excellent solar absorption (>96 % in the 250—2250 nm range). Due to the combined effect of CF morphology and enhanced optical absorption of $CuCo_2S_4$, excellent evaporation rate was achieved, equal to 2.4 $kg·m^{-2}·h^{-1}$, compared to that of CF (1.6 $kg·m^{-2}·h^{-1}$). This work presents the sustainable development of new low-bandgap energy materials from waste plastic and functionalization with carrollite $CuCo_2S_4$ photothermal layer for freshwater production *via* interfacial solar desalination to mitigate the water and plastic crises, thereby enabling the circular economy.

Electronic Supplementary Information

Supplementary material is available in the online version of this article at http://dx.doi.org/10.1007/s40242-024-4091-8.

Acknowledgements

This work was supported by the Marie Skłodowska-Curie Individual Fellowship (No. GA 101027930), and the Italian Ministry of University (MUR) for funding through Progetti di Ricerca Scientifica di Rilevante Interesse Nazionale (No. 2022FNL89Y), the Kempe Foundation, the Knut & Alice Wallenberg Foundation, and the Project of Ca' Foscari University of Venice (SPIN Project), the National Recovery and Resilience Plan (NRRP), Mission 4 Component 2 Investment 1.3, Project NEST.

The authors acknowledge technical support from Mr. Tiziano FINOTTO for the collection of XRD data.

Conflicts of Interest

The authors declare no conflicts of interest.

References

[1] Elsaid K., Kamil M., Sayed E. T., Abdelkareem M. A., Wilberforce T., Olabi A., *Sci. Total Environ.*, **2020**, *748*, 141528.
[2] Karami S., Roghabadi F. A., Maleki M., Ahmadi V., Sadrameli S. M., *Sol. Energy*, **2021**, *225*, 747.
[3] Ni G., Zandavi S. H., Javid S. M., Boriskina S. V., Cooper T. A., Chen G., *Energy Environ. Sci.*, **2018**, *11*, 1510.
[4] Elsheikh A. H., Sharshir S. W., Ali M. K., Shaibo J., Edreis E. M., Abdelhamid T., Du C., Haiou Z., *Sol. Energy*, **2019**, *177*, 561.
[5] Bai B., Yang X., Tian R., Ren W., Suo R., Wang H., *Appl. Therm. Eng.*, **2019**, *163*, 114379.
[6] Wang G., Fu Y., Ma X., Pi W., Liu D., Wang X., *Carbon*, **2017**, *114*, 117.
[7] Fu Y., Wang G., Mei T., Li J., Wang J., Wang X., *ACS Sustain. Chem. Eng.*, **2017**, *5*, 4665.
[8] Jiang F., Liu H., Li Y., Kuang Y., Xu X., Chen C., Huang H., Jia C., Zhao X., Hitz E., Zhou Y., *ACS Appl. Mater. Interfaces*, **2018**, *10*, 1104.
[9] Jiang M., Wang X., Xi W., Zhou H., Yang P., Yao J., Jiang X., Wu D., *J. Chem. Eng.*, **2023**, *461*, 141962.
[10] Cabernard L., Pfister S., Oberschelp C., Hellweg S., *Nat. Sustain*, **2022**, *5*, 139.
[11] Bai H., Liu N., Hao L., He P., Ma C., Niu R., Gong J., Tang T., *Energy Environ. Mater.*, **2022**, *5*, 1204.
[12] Bai H., He P., Hao L., Liu N., Fan Z., Chen B., Niu R., Gong J., *J. Environ. Chem. Eng.*, **2022**, *10*, 108338.
[13] Song C., Zhang B., Hao L., Min J., Liu N., Niu R., Gong J., Tang T., *Green Energy Environ.*, **2022**, *7*, 411.
[14] Zhu J., Huang L., Bao F., Chen G., Song K., Wang Z., Xia H., Gao J., Song Y., Zhu C., Lu F., *Mat. Rep.*: *Energ.*, **2023**, *12*, 100245.
[15] Jiang J., Jiang H., Xu Y., Chen M., Ai L., *Colloids Surf.*, **2022**, *647*, 128960.
[16] Taranova A., Akbar K., Yusupov K., You S., Polewczyk V., Mauri S., Balliana E., Rosen J., Moras P., Gradone A., Morandi V., Moretti E., Vomiero A., *Nat. Commun.*, **2023**, *14*, 7280.
[17] Gao T., Wu X., Owens G., Xu H, L., *Tungsten*, **2020**, *2*, 423.

[18] Chen C., Liu H., Wang H., Zhao Y., Li M., *Nano Energy*, **2021**, *84*, 105868.
[19] Lv F., Miao J., Hu J., Orejon D., *Small*, **2023**, 2208137.
[20] Ibrahim K. B., Shifa T. A., Zorzi S, Sendeku M. G, Moretti E., Vomiero A., *Prog. Mater. Sci.*, **2024**, *20*, 101287.
[21] Ibrahim K. B., Shifa T. A., Bordin M., Moretti E., Wu H. L, Vomiero A., *Small Methods*, **2023**, *7*, 2300348.
[22] Chen X., Liu S., Yang N., Yu R., Wang D., *EcoMat*, **2023**, *5*, 12348.
[23] Wei Y., Wang J., Yu R., Wan J., Wang D., *Angewandte Chemie Intern Edition*, **2019**, *58*, 1422.
[24] Guo M., Balamurugan J., Thanh TD., Kim N. H., Lee J. H., *J. Mater. Chem.*, **2016**, *4*, 17560.
[25] Konwar M., Mahanta B., Patar S., Saikia P., Guha A. K., Borthaku L. J., *ChemistrySelect*, **2022**, *7*, 202203585.
[26] Vadivel S., Paul B., Habibi-Yangjeh A., Maruthamani D., Kumaravel M., Maiyalagan T., *J. Phys. Chem. Solids*, **2018**, *123*, 242.
[27] Li L., Xu J., Ma J., Liu Z., Li Y., *J. Colloid Interface Sci.*, **2019**, *552*, 17.
[28] Zhu G., Zheng P., Wang M., Chen W., Li C., *Inorg. Chem. Front*, **2022**, *9*, 1006.
[29] Ferreira M. L., Santos T. G., Calixto J. M., Lavall R. L., Justino D. D., Gandra F. G., Souza T. D., Ladeira L. O., *Environ. Sci. Pollut. Res. Int.*, **2023**, *30*, 79082.
[30] Peymanfar R., Selseleh-Zakerin E., Ahmadi A., Tavassoli S. H., *Sci. Rep.*, **2021**, *11*, 11932.
[31] Tao F., Zhang Y., Cao S., Yin K., Chang X., Lei Y., Chen X., *Mater. Today Energy*, **2018**, *9*, 285.
[32] Song C., Wang L., Li X., Guo L., Leng Y., Jin X., Ye L., *Inorg. Chem. Commun.*, **2021**, *133*, 108886.
[33] Yang Y., Zhao H., Yin Z., Zhao J., Yin X., Li N., Que W., *Mater. Horiz.*, **2018**, *5*, 1143.
[34] Chen C., Li Y., Song J., Yang Z., Kuang Y., Hitz E., Hu L., *Adv. Mater.*, **2017**, *29*, 1701756.
[35] Yin X., Zhang Y., Xu X., Wang Y., *J. Solid State Chem.*, **2021**, *303*, 122423.
[36] Jiang J., Yang R., Lu X., Ai L., *Desalination*, **2024**, *569*, 117042.